Tunable magnetic exchange springs in semiconductor GdN/NdN superlattices

J. F. McNulty,[1] E.-M. Anton,[1,*] B. J. Ruck,[1] M. Suzuki,[2] M. Mizumaki,[2] and H. J. Trodahl[1]

[1]*MacDiarmid Institute for Advanced Materials and Nanotechnology, School of Chemical and Physical Sciences, Victoria University of Wellington, P.O. Box 600, Wellington 6140, New Zealand*

[2]*Japan Synchrotron Radiation Research Institute, 1-1-1 Kouto, Sayo, Hyogo 679-5198, Japan*

(Received 2 May 2019; revised manuscript received 9 August 2019; published 26 September 2019)

We report twisted magnetization phases, i.e., exchange springs, across interfaces in a semiconducting NdN/GdN superlattice and compare the exchange springs to those reported previously across SmN/GdN interfaces. Like SmN, NdN has an orbital moment larger than and opposing its spin magnetic moment, resulting in exchange-Zeeman competition that in turn precipitates the exchange springs. In contrast to SmN, NdN has a large net magnetic moment, adding more complexity to the exchange-spring behavior. We investigate how different temperatures and applied magnetic fields influence the twisted magnetization using complementary magnetometry and element specific x-ray magnetic circular dichroism. The exchange spring can be driven into two different phases, with either the hard NdN or soft GdN entering the twisted phase. This tunable twisted magnetization in ferromagnetic semiconductors could open up a pathway to control tunneling magnetoresistance in spintronics devices, encouraging further investigation of these new types of exchange springs.

DOI: 10.1103/PhysRevB.100.094441

I. INTRODUCTION

The exchange interaction across an interface between different magnetic materials is well known to result in a variety of magnetic configurations, depending on the details of the magnetic order present in each system. In ferromagnet-antiferromagnet (FM-AFM) systems, interface exchange can lead to the exchange-bias effect, under which the ferromagnetic hysteresis is shifted by an exchange bias field H_{EB} [1], while at the interface of soft and hard FMs, domain-wall-like magnetic ordering can be formed in the soft layer (an exchange spring) due to competing Zeeman and exchange interactions [2] [Fig. 1(b)]. The details of the resulting exchange springs are further influenced by bulk and surface anisotropies, while chiral exchange interactions play a role in some systems [3,4]. Interface exchange effects have been almost exclusively studied in metallic systems, where applications have been found in hard-drive read heads, spin filters, and giant-magnetoresistance devices. In contrast, current understanding of interface exchange in ferromagnetic semiconductors is more limited, although they offer the possibility of controlling spin-polarized currents in engineered spintronics devices.

Among the rare-earth nitride (REN) series, there are many intrinsic ferromagnetic semiconductors, which have shown promise for low-temperature spintronics applications [5–10], as well as displaying unusual interface exchange. The rare-earth nitrides are chemically very similar, and all share the cubic rocksalt structure with similar lattice constants, making them epitaxy compatible with each other. Their magnetic properties, however, vary widely across the series [5]. This makes the rare-earth nitrides an ideal model system to study magnetic interface effects without complications arising from differing crystal lattice properties.

From a magnetician's point of view the light rare-earth nitrides NdN [11] and SmN [12–15] are particularly interesting. In the first half of the rare-earth series the strong spin-orbit coupling of the $4f$ shell forces antiparallel alignment of the total $4f$ spin $m_S = -2\mu_B\langle S_z\rangle$ and orbital $m_L = -\mu_B\langle L_z\rangle$ magnetic moments, with the magnitude of the orbital moment m_L exceeding that of m_S in NdN and SmN [Fig. 1(a)]. In this sense we refer to NdN and SmN as "orbital-dominant" ferromagnets, in contrast to spin-dominant transition-metal ions and heavy rare earths. It is the antiparallel alignment between m_L and m_S which allows for an unusual interface exchange in heterostructures.

Previous work shows that this orbital-dominant vs spin-only contrast results in an exchange spring (or twisted magnetization) formation in the SmN layer of a SmN/GdN bilayer [13]. In this system, the SmN Zeeman coupling competes with interface exchange with the spin-only GdN, resulting in an unusual form of exchange spring for two reasons. First, the SmN, in which the twisted magnetization phase develops, is a magnetically hard material at low temperatures ($H_C > 6$ T at 2 K [16]), while GdN is a soft magnet with a very small coercive field ($H_C \leqslant 10$ mT) [17]. By contrast conventional exchange springs generally develop within the soft ferromagnetic films coupled to hard layers [Fig. 1(b)] [2,18,19]. Second, the SmN/GdN is semiconducting, in contrast to nearly all exchange-spring systems, which are metallic. The only notable exception of which we are aware is a system in which the dilute magnetic semiconductor $Ga_{1-x}Mn_xAs$ was exchange coupled to a hard ferromagnetic metal, and a large tunneling magnetoresistance due to exchange-spring formation in the soft $Ga_{1-x}Mn_xAs$ was observed [20–22]. Dilute magnetic semiconductors have limited potential compared to systems using intrinsic ferromagnetic semiconductors like the

*eva.anton@vuw.ac.nz

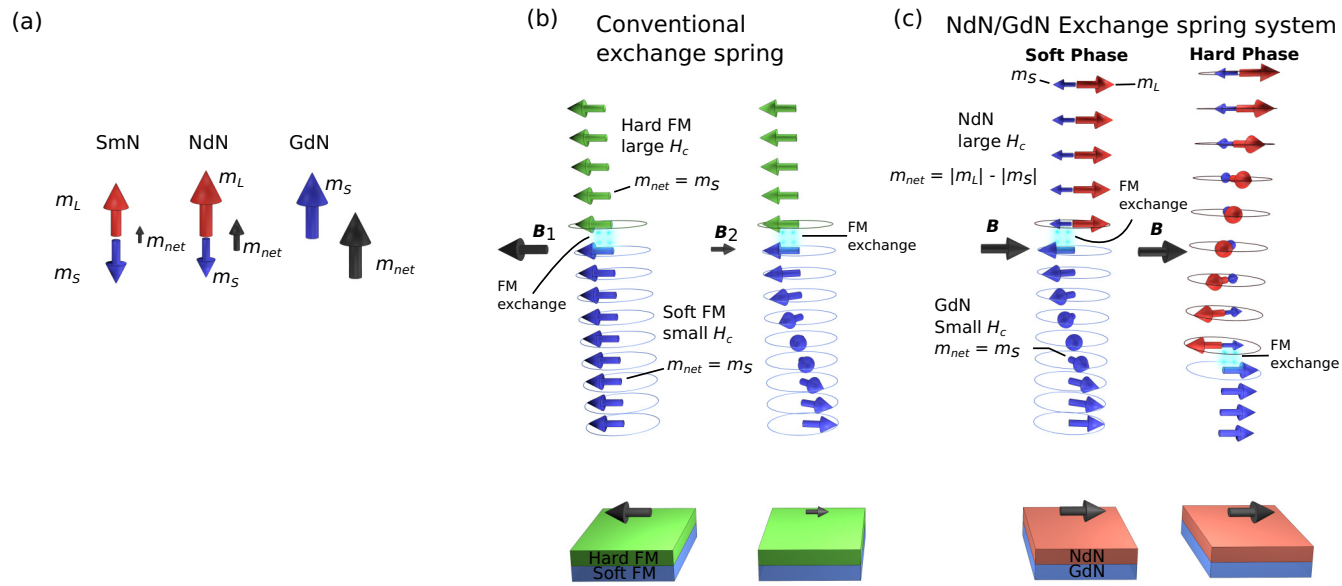

FIG. 1. (a) Schematic of magnetic moments in trivalent Nd, Sm, and Gd ions, where $m_L = -\mu_B\langle L_z\rangle$, $m_S = -2\mu_B\langle S_z\rangle$, and $m_{\rm net} = m_L + m_S = -\mu_B\langle L_z + 2S_z\rangle$. The orbital moment is larger in NdN and SmN and determines the direction of the net magnetic moment, whereas Gd has a purely spin moment with its f^7 configuration and $S = J = 7/2$, $L = 0$ state. (b) A conventional exchange spring is formed by exploiting the different switching fields of hard and soft ferromagnetic layers. (c) The NdN/GdN exchange spring results from an orbital-dominant layer (NdN), in which the spins are forced antiparallel to an applied magnetic field $\boldsymbol{B}$, and a conventional ferromagnetic layer (GdN), in which spins align with the magnetic field. Depending on the balance of exchange, Zeeman, and magnetocrystalline anisotropy energies in each material, an exchange spring forms in the soft GdN layer (soft phase) or the hard NdN layer (hard phase).

RENs, which, in principle, allow for entirely semiconducting heterostructures, with the ability to independently tune electrical and magnetic properties. Exchange springs are essentially engineered domain walls, depending on layer thickness and external magnetic fields, and when combined with the independently tunable electric and magnetic properties of RENs, an unprecedented opportunity to probe the interplay between inhomogeneous magnetic order and spin-polarized transport in semiconductors is available.

Here we investigate a NdN/GdN superlattice to establish that this system hosts twisted magnetization phases. In contrast to the near-zero moment SmN, NdN has a stronger net magnetic moment of $1\mu_B$ per ion in strained thin films, increasing to $2.1\mu_B$ per ion in bulk samples [11]. Additionally, the coercive field of NdN, while still large with 1.5 T at temperatures of 5 K, is nonetheless much smaller than the enormous >6 T in SmN. At 15 K, the coercive field of NdN is only 0.75 T, and at 30 K it is only 0.25 T, signaling a rapid decrease in the magnetocrystalline anisotropy when approaching T_C of 35–43 K [11]. The orbital-dominant magnetism in NdN suggests that it might also develop exchange-spring behavior similar to SmN, but the distinct differences in their magnetic properties will affect the nature of the twisted phases. It is the aim of this study to gain insight into these inhomogeneous magnetic phases in the NdN/GdN system. In contrast to SmN/GdN, we find more complex magnetic phases in this NdN/GdN system. We expected to find a twisted magnetization phase in the hard NdN layer, while the much larger GdN magnetization is kept rigidly aligned with the field. This behavior found for the SmN/GdN system is indeed observed at higher temperatures and lower maximum applied fields and corresponds to the hard phase in Fig. 1(c). For lower temperatures and higher maximum applied fields, we observe a new kind of twisted magnetization phase, where with decreasing field the soft GdN first develops exchange springs, later followed by the hard NdN at negative fields [here referred to as the soft phase, Fig. 1(c)].

II. EXPERIMENTAL DETAILS

The sample for which we report results was a $10 \times$ (10 nm NdN/10 nm GdN) superlattice grown on a GaN(0001) buffer layer with a sapphire(0001) substrate. The growth method was molecular beam epitaxy in a Thermionics ultrahigh-vacuum chamber in a N_2 pressure of 2×10^{-4} Torr. NdN and GdN were evaporated with an electron gun facing the substrate without tilt at a rate of 0.1 to 0.2 Å/s. It was capped with a GaN layer of approximately 50-nm thickness. X-ray diffraction indicated polycrystalline GdN and NdN layers.

In-plane magnetization measurements were carried out via a Quantum Design superconducting quantum interference device (SQUID) and vibrating sample magnetometer. For zero-field cooled (ZFC) measurements, the sample was first cooled to 5 K in zero field and subsequently measured in a field of 250 Oe as the temperature was increased, while for the field cooled (FC) measurements the magnetization was measured with decreasing temperature in a field of 250 Oe.

L-edge x-ray absorption and x-ray magnetic circular dichroism (XMCD) were measured at BL39XU at the SPring-8 synchrotron radiation facility. The x rays and colinear magnetic field were directed at 18° from grazing incidence. XMCD was measured at a fixed magnetic field while switching the x-ray polarization. The resulting XMCD spectra were

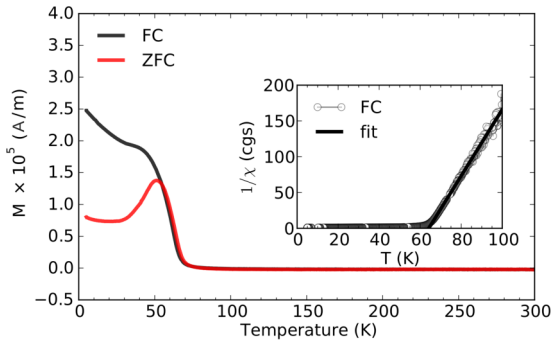

FIG. 2. Temperature-dependent magnetization of the NdN/GdN superlattice in a 250-Oe field, showing both field-cooled (FC) and zero-field cooled (ZFC) measurements. The inset shows the Curie-Weiss behavior in the inverse susceptibility taken from the FC measurement.

normalized to the edge jump measured by x-ray absorption spectroscopy (XAS). The detection scheme was partial fluorescence yield using a silicon drift detector, where the $L_{\alpha 1}$ and $L_{\beta 1}$ fluorescence is measured when probing the L_3 and L_2 edges, respectively. The long mean free path of x rays at these energies ensures that the XMCD spectra represent the average signal from the full thickness of the film. Saturation, self-absorption, and orbital contraction effects are known to prevent the application of sum rules at the rare-earth L edges [23,24], but they do not affect the shape of the hysteresis loops presented here. The shapes of the XMCD spectra taken at different fields are identical within the experimental resolution, with only the amplitude changing.

III. RESULTS AND DISCUSSION

A. Magnetization

We begin by examining the overall magnetization of the superlattice measured via SQUID magnetometry, displayed in Fig. 2. Both FC and ZFC curves show a rapidly increasing magnetization as the temperature falls below ≈70 K, corresponding to the onset of ferromagnetism in the GdN layers. A Curie-Weiss fit $\chi = A/(T - \theta_p) + \chi_0$ with a constant background χ_0 to account for the diamagnetic substrate contribution yields a paramagnetic Curie temperature of $\theta_p = 65 \pm 1$ K, also visible in the inverse susceptibility $(\chi - \chi_0)^{-1}$ shown in the inset of Fig. 2. This Curie temperature is typical of polycrystalline GdN samples and indicates that the NdN contribution to the paramagnetic signal is weak. Indeed, the smaller paramagnetic moment of NdN ensures that its signal at 85 K is ≈15 times weaker, consistent with the data showing a paramagnetic response dominated by GdN.

The field-cooled magnetization below 50 K shows a more complex behavior influenced by interface exchange. Bulk GdN shows a saturating magnetization at low temperatures, yet here the FC magnetization has a significant negative slope below ≈35 K. This suggests interface exchange of the GdN with NdN, which has a T_C of between 35 and 43 K [11]. The nearly linear slope of the FC curve below 25 K is not characteristic of either NdN or GdN thin films approaching saturation, implying GdN-NdN interface coupling competes

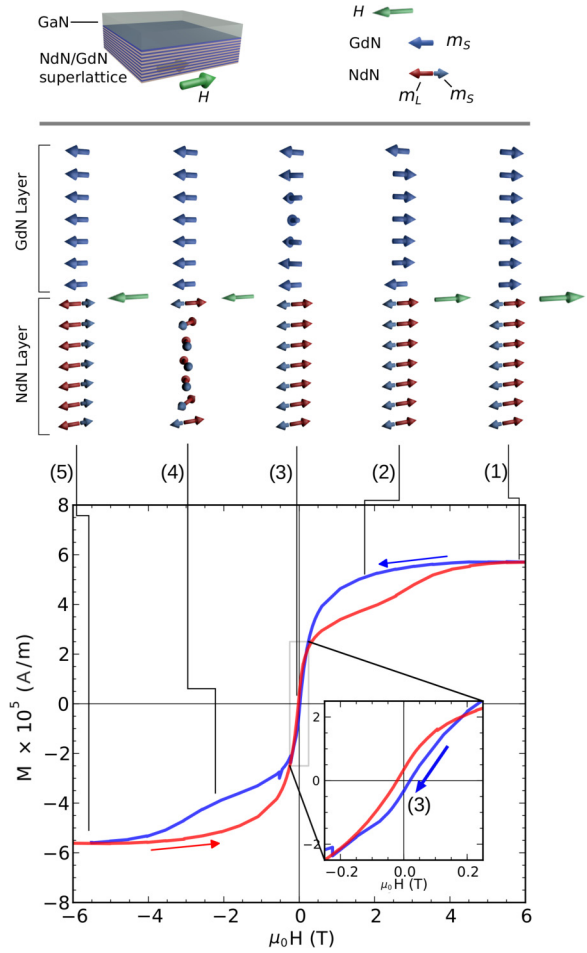

FIG. 3. *M*-*H* plot for the NdN/GdN superlattice at 5 K, with field in plane, after zero-field cooling. Sketches of the various moment arrangements (1)–(5) in the GdN and NdN layers are given as the field decreases from saturation at 6 T; the sketches should thus be read from right to left. The small dip at −0.5 T in the decreasing-field loop is a measurement artifact.

with the tendency of the individual GdN and NdN layers to saturate as $T \to 0$.

To gain deeper insight into the complex magnetic behavior in NdN/GdN, we performed field-dependent magnetization measurements at different temperatures. The hysteresis loop displayed in Fig. 3, with both NdN and GdN deep in their ferromagnetic phase, shows especially striking effects of the interlayer exchange. The solid blue curve, taken in a field decreasing from 6 T, is qualitatively similar to a conventional ferromagnet until the field is close to zero, where it finally has a *negative* remanent magnetization, $M_R = -0.3 \times 10^5$ A/m. The coercive field is then also necessarily negative, with value $\mu_0 H_C = -0.02$ T. The negative signs of H_C and M_R signal that the net magnetization of the superlattice switches sign while the magnetic field is still positive. Furthermore, the field-reducing curve shows an apparent approach to saturation at ∼−1 T before a steepening slope at −2 T, with similar features in the red (field-increasing) curve above 2 T. None of these features can be interpreted within a simple model of noninteracting ferromagnetic layers.

We can make some estimates in order to understand why the magnetization is negative at zero field, as in Fig. 3. At 5 K and an applied field of 6 T we may assume that the moments are close to their saturation values, approximately $7\mu_B$ per ion for GdN and $0.9\mu_B$–$2.1\mu_B$ per ion for NdN [11]. In this case the NdN moment is only ≈15%–30% of the GdN moment. The ratio of remanent to saturation magnetization M_S of the total superlattice magnetization is given by $M_R = -0.1M_S$, a value small enough to rule out full magnetization reversal of either GdN or NdN as an explanation for the small, negative M_R. Rather, the negative M_R signals that the GdN layers—with their much larger magnetic moments—have their magnetization partially reversed when $H = 0$. The NdN layers, with a large coercive field at 5 K (≈1.5 T in bulk NdN [11]), are unable to reverse due to their large anisotropy energy, whereas GdN has negligible anisotropy. The ferromagnetic interface exchange, *which acts purely between spins*, causes interfacial GdN to undergo a partial magnetization reversal while the NdN remains fixed, acting as a hard anchoring layer. The unusual orbital-dominant moment of NdN, with spin moment antiparallel to the net moment, results in an *antiferromagnetic* alignment of the GdN and NdN net magnetizations, which is really due to *ferromagnetic* interface exchange between spin moments.

The situation is sketched in the top panel of Fig. 3, where a single bilayer of the NdN/GdN superlattice is depicted, with the magnetization of each layer sketched in configurations corresponding to points on the blue (decreasing-field) *M-H* curve. Starting in configuration 1 in Fig. 3, at 6 T, the GdN and NdN layers have their magnetization aligned fully along the field. Note that this incurs an energetic cost associated with antiparallel alignment of Gd and Nd spins across the interface. Upon decreasing the field to configuration 2, the interface-adjacent GdN layers react to ferromagnetic exchange with the NdN and thus reverse their direction. Upon reaching zero field (configuration 3), the NdN maintains its alignment, while the GdN alignment is dominated by interface exchange. The GdN magnetization reversal nucleates from the interfaces, and a twisted magnetization is formed such that the net magnetization of the GdN is negative and large enough to make the global superlattice magnetization negative. As the field becomes negative in configuration 4, the GdN magnetization becomes nearly fully aligned with the field, and the innermost NdN layers reverse their magnetization due to the large Zeeman interaction, now forming a twisted magnetization in that layer. Finally, when the field reaches −6 T in configuration 5, the NdN magnetization and GdN are both fully aligned by the field, largely overriding the interface exchange interaction. The process is symmetric upon increasing the field from this point (red curve).

An alternative explanation of the negative remanent magnetization resulting from interdiffusion at the NdN/GdN interface is unlikely for the following reasons. Complete interdiffusion can be ruled out because of the well-defined transitions corresponding to both GdN and NdN T_C's, for example, visible at the GdN T_C in Fig. 2. In Fig. 4 the coercive fields for magnetic hysteresis loops show a clear crossover from negative to positive remanent magnetization between 20 and 35 K, coinciding with the NdN T_C. If the negative remanent magnetization was due to diffusion, we would expect this changeover to happen at a higher temperature between the NdN and GdN T_C's. Partial interdiffusion cannot be ruled out, but its effect has to be small compared to the effect of the twisted magnetization. In Fig. 3, the size of the hump in between steps 3 and 4 with decreasing field is determined by the difference of the NdN magnetization being antiparallel to the GdN magnetization and the magnetizations being parallel (configuration 5). An estimate which takes the sum and difference of M_{GdN} and M_{NdN} to be equal to the top and bottom of the hump yields a ratio $M_{\mathrm{NdN}}/M_{\mathrm{GdN}}$ in the range of 0.1 to 0.2, taking into account uncertainty. This is close to the ratio of the NdN to GdN moment of 0.15 to 0.30, with the lower value corresponding to thin films grown in a fashion similar to that in this study [11]. This fits in well with our model where the gradual unwinding of the magnetization results in a slope change and a hump in the magnetization.

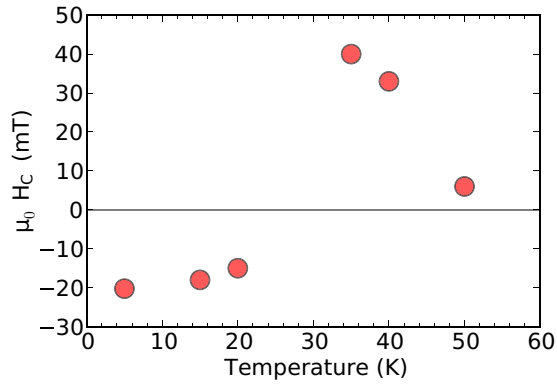

FIG. 4. The coercive fields for magnetic hysteresis loops taken at temperatures from 5 to 50 K show a crossover from negative to positive remanent magnetization between 20 and 35 K, coinciding with the NdN T_C, which is ≈35 K.

B. XMCD investigation

In this section we make use of the element-specific nature of XMCD to shed light on the individual behaviors of the GdN and NdN layers in the superlattice in a regime at higher temperature and lower magnetic fields than in the previous section. In this regime the GdN and NdN have different behaviors and can be said to lie in a different phase. The origin of these two phases is related to the magnetic anisotropy of the NdN layers. At 5 K the coercive field of NdN is about 1.5 T, while in GdN it is of the order of 0.01 T. Because of the rather low NdN T_C, the anisotropy energy decreases significantly with rising temperature, so that XMCD measurements at 16 and 30 K feature a NdN anisotropy that is relatively small, and the NdN is then dominated by the interface exchange coupling with GdN.

Figure 5 shows the Gd and Nd L_2-edge spectra taken in a field of 1.2 T after field cooling in the same field at temperatures of 16 and 30 K. The sign of the Gd-edge XMCD spectra is as reported for GdN films [25,26] and for a SmN/GdN superlattice [13], signaling that the spin magnetic moment on the Gd $4f$ shell is aligned parallel to the field under these conditions. In contrast the sign of the Nd spectra signals an antiparallel configuration of spin and magnetic moments, exactly as seen also with XMCD on homogeneous

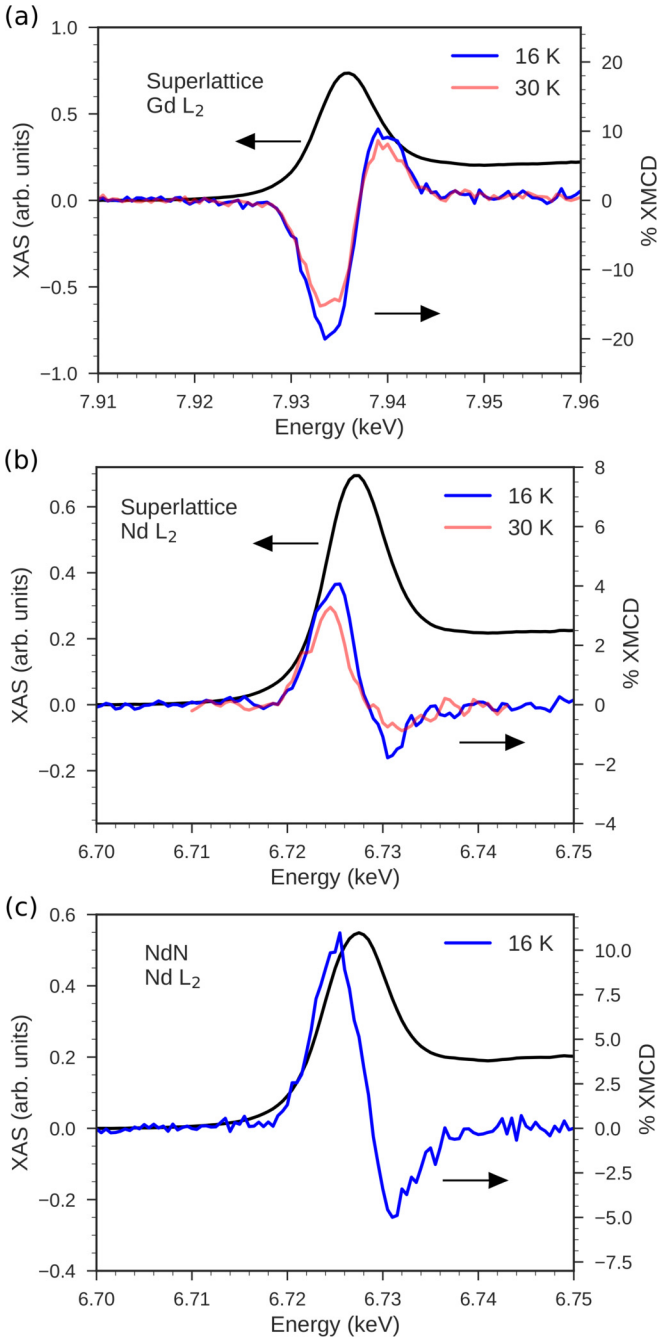

FIG. 5. XAS and XMCD spectra from the NdN/GdN superlattice at (a) the Gd L_2 edge with $T = 16$ K and 30 K. (b) Nd L_2 edge XAS and XMCD spectra for the NdN/GdN superlattice at 16 and 30 K and (c) the homogeneous NdN sample at 16 K. The spectra were measured in 1.2 T after field cooling in the same field.

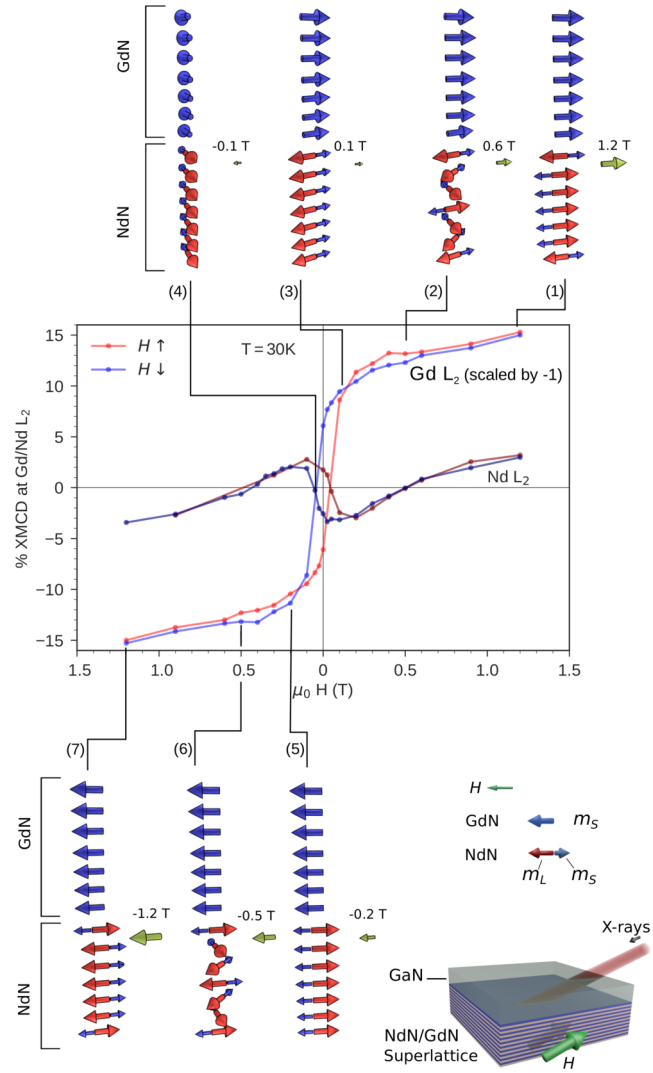

FIG. 6. XMCD hysteresis measured at both Gd and Nd L_2 edges where the sign has been chosen to correspond to the net magnetization within respective GdN and NdN layers. The Gd L_2 curve was measured only for increasing field; thus the blue curve is a mirrored version of the red one. Sketches of moments correspond to the blue curves for decreasing H.

NdN [Fig. 5(c)] [11]. A reduction in the Nd L_2 XMCD signal by a factor of 2 in the superlattice suggests that the inner NdN planes within the NdN layers are Zeeman dominated, while the interface-adjacent layers have their magnetization reversed by exchange with GdN.

We next turn to field-dependent XMCD measurements to investigate hysteretic effects independently within the GdN and NdN layers. The field dependence of the XMCD amplitude at the Gd L_2 and Nd L_2 edges is shown for a temperature of 30 K in Fig. 6. Note that the ordinate scale is chosen to correspond to the net magnetization, so the sign is *opposite* that of the spin magnetic moment in NdN. Thus at the largest fields both layers are shown to have a net magnetization aligned with the applied field.

Examining the Gd L_2 XMCD hysteresis, it is seen that both the remanent magnetization and coercive field are positive, in contrast to the magnetization data taken at 5 K (Fig. 3). In the 5 K magnetization data, it is the NdN layers that pin the GdN magnetization, which is clearly not the case here. Instead, at this higher temperature the Nd L_2 XMCD hysteresis demonstrates that it is the NdN layers which are pinned by the GdN magnetization. The reason for this reversal is that at 30 K the NdN anisotropy is significantly diminished [11], so that the GdN layers' Zeeman interaction is dominant. The XMCD data in Fig. 6 thus signal a scenario much different from the one implied by the hysteresis shown in Fig. 3; here the twisted

phase develops in the NdN layers, while the low-temperature magnetization data signal a GdN layer twisted magnetization phase.

It is also clear that the GdN hysteresis loop self-intersects at approximately ±0.1 and ±0.5 T. This is a signature of exchange coupling with NdN. As the field is decreased from 1.2 T, the Zeeman coupling of the GdN weakens, and the NdN exchange exerts some influence, although not enough to invert the GdN completely. One notices, however, that in contrast to the low-temperature magnetization data of Fig. 3, the magnetization with *decreasing* field is lower in the XMCD hysteresis. The shape of the Gd L_2 hysteresis makes it clear that it behaves largely as a homogeneous GdN sample would, with perturbations from this behavior due to the NdN exchange coupling.

The possible magnetization configurations determined from the XMCD hysteresis are shown as sketches 1–6, in the direction of decreasing magnetic field. At position 1, where $\mu_0 H = 1.2$ T, the NdN and GdN layers are in the Zeeman-dominated regime; that is, the Zeeman energy in both NdN and GdN is greater than interface exchange or anisotropy energies. As the field decreases to position 2, the GdN layers are still Zeeman dominated, while the NdN film is dominated by interface exchange. As the Zeeman energy of the NdN decreases, the exchange spring nucleates at the interface, forming a symmetric exchange spring or twist, which results in a zero average magnetization in the NdN layers at about 0.5 T. At position 3 the NdN layers have been fully "twisted" by interface exchange, such that the magnetization is now negative, and the GdN spins are still largely aligned, parallel to the field. After the field becomes negative (positions 4 and 5), the NdN layer magnetization rotates with the GdN layer. As the field increases in magnitude to position 6, the NdN Zeeman coupling begins to compete with the interface exchange, which still strongly couples the NdN, resulting in the twisted phase nucleating from the center of the NdN layers. By position 7, the field becomes large enough that both NdN and GdN layers are in the Zeeman-dominated regime.

Figure 7 shows an additional 16 K hysteresis loop extracted from XMCD at the Nd L_2 edge, with the 30 K data added for comparison. The 16 K data show the same characteristics as the 30 K measurement, although with a larger amplitude expected at lower temperature. Thus the exchange spring developing at 16 K is expected to follow the same mechanism as described for the 30 K data.

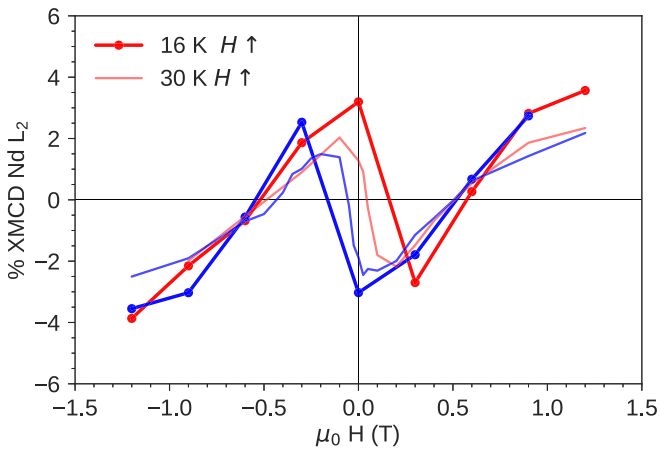

FIG. 7. Comparison of the Nd L_2 hysteresis from the NdN/GdN superlattice measured at 16 and 30 K. Red and blue curves denote measurements with H increasing and decreasing, respectively.

C. Magnetic phase diagram

The preceding sections have clearly demonstrated that in the NdN/GdN superlattice the unique interface exchange coupling produces complex magnetic structures. The twisted phase due to exchange-Zeeman competition manifests in two ways: in the low-temperature SQUID magnetization data we saw that the GdN magnetization switched first, while the NdN magnetization reversed fully in very large negative fields. In contrast, the XMCD hysteresis at higher temperatures showed that the NdN magnetization reverses first, followed by the GdN only after the field reverses. The twisted phase can be characterized as follows: a "soft phase" where the soft GdN layers pass through a twisted phase and reverse before the field does, and a "hard phase" where the hard NdN layers enter a twisted phase and reverse before the field reaches zero. The boundary between these phases depends on both temperature and the maximum applied field during field cooling. A similar situation is found in the $DyFe_2/YFe_2$ system, where $DyFe_2$ is a hard ferrimagnet and YFe_2 is a weak ferrimagnet. In that case there is an antiferromagnetic interface exchange which leads to similar soft and hard phases depending on the temperature [19,27].

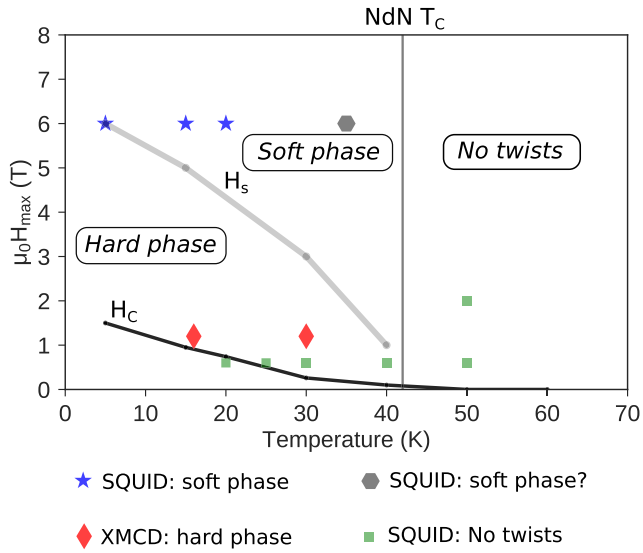

FIG. 8. A phase diagram summarizing the findings of all available XMCD and SQUID measurements of the twisted magnetic phases in the NdN/GdN superlattice. Blue stars represent measurements demonstrating twisted magnetization in the soft phase; red diamonds show twisted magnetization in the hard phase. In the measurements represented by green squares no evidence of twisted magnetization is found. The gray hexagon represents a measurement likely in the soft phase, but without the characteristic negative M_R (see text for explanation). H_s represents the approximate field required to saturate the magnetization in bulk NdN and is the likely boundary between the soft and hard phases. H_C is the coercive field of NdN.

Figure 8 shows a phase diagram taken from all available magnetization and XMCD measurements, with the maximum applied field $\mu_0 H_{\max}$ plotted along the vertical axis. The soft phase, in which the GdN enters a twisted phase, is located in the top left quadrant, with the maximum applied field at 6 T. The gray hexagon at 35 K represents a hysteresis in SQUID magnetization data at that temperature, which shows a positive M_R, although it is only 25% of the saturation magnetization at high field. At this point GdN likely enters a twisted phase, but the interface exchange is not strong enough to produce a negative magnetization in the GdN layer. The line H_s represents the saturation field of bulk NdN and corresponds approximately to the boundary between the soft and hard phases. It seems that a field of at least H_s must be applied to align the NdN magnetization to a sufficient degree for producing a rigid pinning layer for the GdN layers to develop a twisted phase. The green squares represent SQUID measurements which show no apparent evidence of a twisted phase. Below the NdN T_C, this is most likely because the maximum applied field is not large enough to sufficiently align the NdN layers. Above the NdN T_C, interface exchange may take place with the GdN, but there is no intralayer NdN exchange to support any twisted phase, even in large fields.

IV. SUMMARY

The combination of magnetization measurements and the element-specific tool of XMCD paint a complex picture of the NdN/GdN superlattice system. The exchange-spring behavior in a NdN/GdN superlattice results from competition between the orbital-dominant NdN ferromagnetism, which aligns the spin magnetic moment antiparallel to an applied field, and the GdN spin magnetic moment's field-parallel alignment. The competition between the exchange interaction of the opposing spins across the interface and the Zeeman interaction then drives an exchange-spring configuration. Varying the temperature and maximum applied field reveals two contrasting regimes corresponding to exchange-spring formation in either NdN or GdN layers. For higher maximum applied fields and lower temperatures we observe a twisted magnetization phase involving both layers. Following a hysteresis loop with decreasing fields, the soft GdN layer enters a twisted magnetization phase before the GdN spins fully reverse at a negative field. At that stage, the hard NdN layer starts its magnetization reversal, developing a twisted magnetization until saturation is reached. In the other regime, at lower maximum applied fields and higher temperatures, the twisted magnetization follows the mechanism described for SmN/GdN before, where the hard magnetic layer, NdN, enters a twisted phase. The controlling parameter for selecting the two phases is primarily the magnetocrystalline anisotropy in NdN, which vastly exceeds that in GdN at low temperatures but falls to nearly zero as the temperature rises towards the NdN T_C. This tunable exchange-spring behavior in a ferromagnetic semiconductor system could lead to interesting effects in the magnetoresistance, with potential application in future spintronics devices.

ACKNOWLEDGMENTS

We are grateful for financial support from the NZ FRST (Grant No. VICX0808) and the Marsden Fund (Grant No. 08-VUW-030). The MacDiarmid Institute is supported by the New Zealand Centres of Research Excellence Fund. The synchrotron radiation experiments were performed at SPring-8 with the approval of the Japan Synchrotron Radiation Institute (JASRI; Proposal No. 2014B1310/BL39XU).

[1] J. Nogués and I. K. Schuller, J. Magn. Magn. Mater. **192**, 203 (1999).
[2] E. E. Fullerton, J. S. Jiang, M. Grimsditch, C. H. Sowers, and S. D. Bader, Phys. Rev. B **58**, 12193 (1998).
[3] A. Thiaville and A. Fert, J. Magn. Magn. Mater. **113**, 161 (1992).
[4] U. K. Rößler, A. N. Bogdanov, and C. Pfleiderer, Nature (London) **442**, 797 (2006).
[5] F. Natali, B. J. Ruck, N. O. V. Plank, H. J. Trodahl, S. Granville, C. Meyer, and W. R. L. Lambrecht, Prog. Mater Sci. **58**, 1316 (2013).
[6] K. Senapati, M. G. Blamire, and Z. H. Barber, Nat. Mater. **10**, 849 (2011).
[7] H. Warring, B. Ruck, H. Trodahl, and F. Natali, Appl. Phys. Lett. **102**, 132409 (2013).
[8] A. Pal, K. Senapati, Z. H. Barber, and M. G. Blamire, Adv. Mater. **25**, 5581 (2013).
[9] P. K. Muduli, A. Pal, and M. G. Blamire, Phys. Rev. B **89**, 094414 (2014).
[10] D. Massarotti, A. Pal, G. Rotoli, L. Longobardi, M. Blamire, and F. Tafuri, Nat. Commun. **6**, 7376 (2015).
[11] E.-M. Anton, J. F. McNulty, B. J. Ruck, M. Suzuki, M. Mizumaki, V. N. Antonov, J. W. Quilty, N. Strickland, and H. J. Trodahl, Phys. Rev. B **93**, 064431 (2016).
[12] E.-M. Anton, B. J. Ruck, C. Meyer, F. Natali, H. Warring, F. Wilhelm, A. Rogalev, V. N. Antonov, and H. J. Trodahl, Phys. Rev. B **87**, 134414 (2013).
[13] J. F. McNulty, E.-M. Anton, B. J. Ruck, F. Natali, H. Warring, F. Wilhelm, A. Rogalev, M. M. Soares, N. B. Brookes, and H. J. Trodahl, Phys. Rev. B **91**, 174426 (2015).
[14] E.-M. Anton, S. Granville, A. Engel, S. V. Chong, M. Governale, U. Zülicke, A. G. Moghaddam, H. J. Trodahl, F. Natali, S. Vézian, and B. J. Ruck, Phys. Rev. B **94**, 024106 (2016).
[15] J. F. McNulty, B. J. Ruck, and H. J. Trodahl, Phys. Rev. B **93**, 054413 (2016).
[16] C. Meyer, B. J. Ruck, J. Zhong, S. Granville, A. R. H. Preston, G. V. M. Williams, and H. J. Trodahl, Phys. Rev. B **78**, 174406 (2008).
[17] B. M. Ludbrook, I. L. Farrell, M. Kuebel, B. J. Ruck, A. R. H. Preston, H. J. Trodahl, L. Ranno, R. J. Reeves, and S. M. Durbin, J. Appl. Phys. **106**, 063910 (2009).

[18] E. Goto, N. Hayashi, T. Miyashita, and K. Nakagawa, J. Appl. Phys. **36**, 2951 (1965).
[19] G. B. G. Stenning, G. J. Bowden, P. A. J. de Groot, G. van der Laan, A. I. Figueroa, P. Bencok, P. Steadman, and T. Hesjedal, Phys. Rev. B **91**, 094403 (2015).
[20] M. Zhu, M. J. Wilson, P. Mitra, P. Schiffer, and N. Samarth, Phys. Rev. B **78**, 195307 (2008).
[21] M. J. Wilson, M. Zhu, R. C. Myers, D. D. Awschalom, P. Schiffer, and N. Samarth, Phys. Rev. B **81**, 045319 (2010).
[22] T. Dietl and H. Ohno, Rev. Mod. Phys. **86**, 187 (2014).
[23] G. van der Laan and A. I. Figueroa, Coord. Chem. Rev. **277–278**, 95 (2014).
[24] M. van Veenendaal, J. B. Goedkoop, and B. T. Thole, Phys. Rev. Lett. **78**, 1162 (1997).
[25] F. Leuenberger, A. Parge, W. Felsch, F. Baudelet, C. Giorgetti, E. Dartyge, and F. Wilhelm, Phys. Rev. B **73**, 214430 (2006).
[26] V. N. Antonov, B. N. Harmon, A. N. Yaresko, and A. P. Shpak, Phys. Rev. B **75**, 184422 (2007).
[27] K. Dumesnil, C. Dufour, P. Mangin, A. Rogalev, and F. Wilhelm, J. Phys.: Condens. Matter **17**, 215 (2005).